Electronic Supplementary Information (ESI)

The Pivotal Alkyne Group in the Mutual Size-Conversion of Au_9 with Au_{10} Nanoclusters

Xiaohang Wu,[a] Ying Lv,[a] Yuyuan Bai,[a] Haizhu Yu,*[ab] and Manzhou Zhu[ab]

[a.]Anhui Province Key Laboratory of Chemistry for Inorganic/Organic Hybrid Functionalized Materials, Key Laboratory of Structure and Functional Regulation of Hybrid Materials of Ministry of Education, Anhui University, Hefei, Anhui, 230601 P. R. China.
Email: yuhaizhu@ahu.edu.cn.
[b.]Institute of Physical Science and Information Technology, Anhui University, Hefei, Anhui, 230601 P. R. China.

Table S1. Selected structural parameters for the single crystal structure (**Au_9/Au_{10}-crys**), full-ligands protected structure (**Au_9^T/Au_{10}^T-full**), and simplified ligands protected structures (**Au_9^T/Au_{10}^T**).

	BD^{Au-Au}	$DA^{8-9-10-3}$	$DA^{7-8-9-10}$	$DA^{2-7-8-9}$	$DA^{3-2-7-8}$	$DA^{10-3-2-7}$	$DA^{9-10-3-2}$
Au_9-crys	2.776	29.6	296.9	79.5	296.7	21.4	354.2
Au_9^T-full	2.866	22.3	302.3	76.1	298.7	17.5	0.4
Au_9^T	2.850	20.7	303.5	76.0	299.5	17.2	1.2
Au_{10}-crys	2.867	41.8	285.0	85.6	287.3	31.3	28.8
Au_{10}^T-full	2.986	40.7	290.6	80.0	292.3	32.0	328.3
Au_{10}^T	2.942	58.0	283.9	73.7	299.7	38.5	321.3

Note: The average Au-Au bond distances (BD^{Au-Au}) and dihedral angles ($DA^{a-b-c-d}$) are given in angstrom and degree, respectively. The calculation method on **Au_9^T/Au_{10}^T-full** is the same as that of the modeling **Au_9^T/Au_{10}^T.**

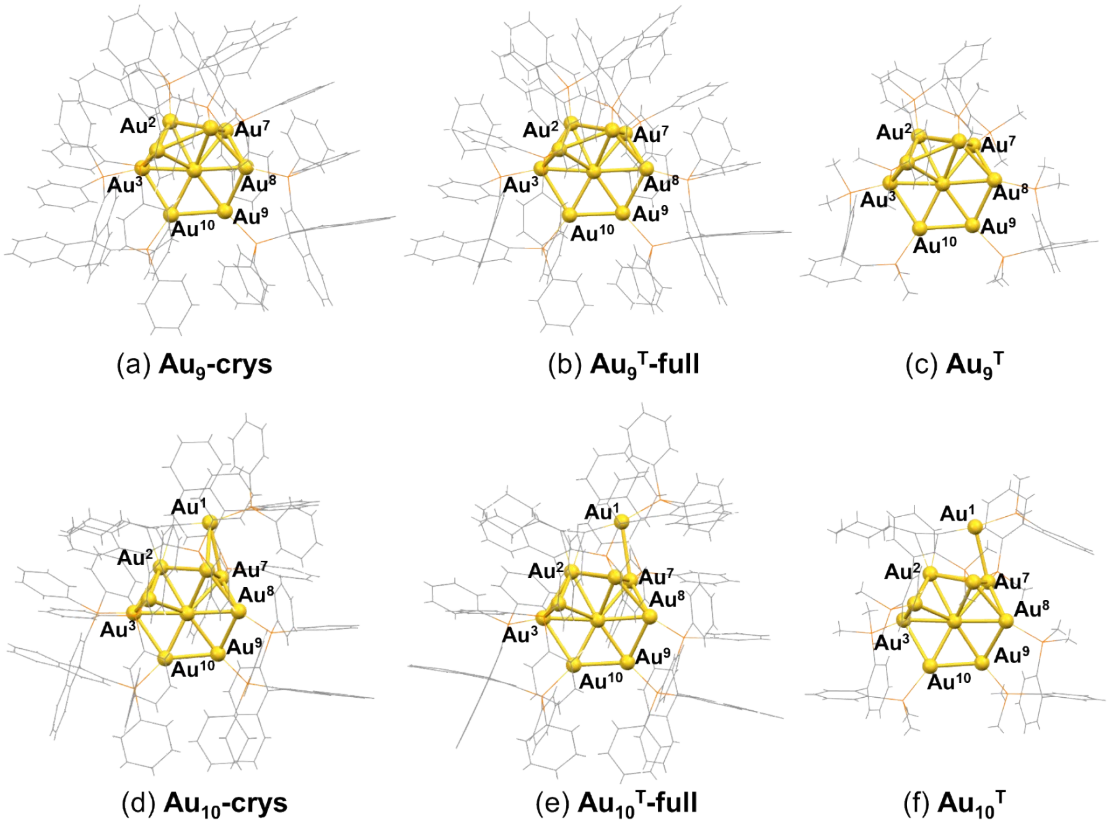

Figure S1. The geometries of the single crystal structures of **Au_9^T/Au_{10}^T-crys**, $Au_{9/10}$ cluster with full ligands (**Au_9^T/Au_{10}^T-full**), and $Au_{9/10}$ cluster with simplified ligands (**Au_9^T/Au_{10}^T**).

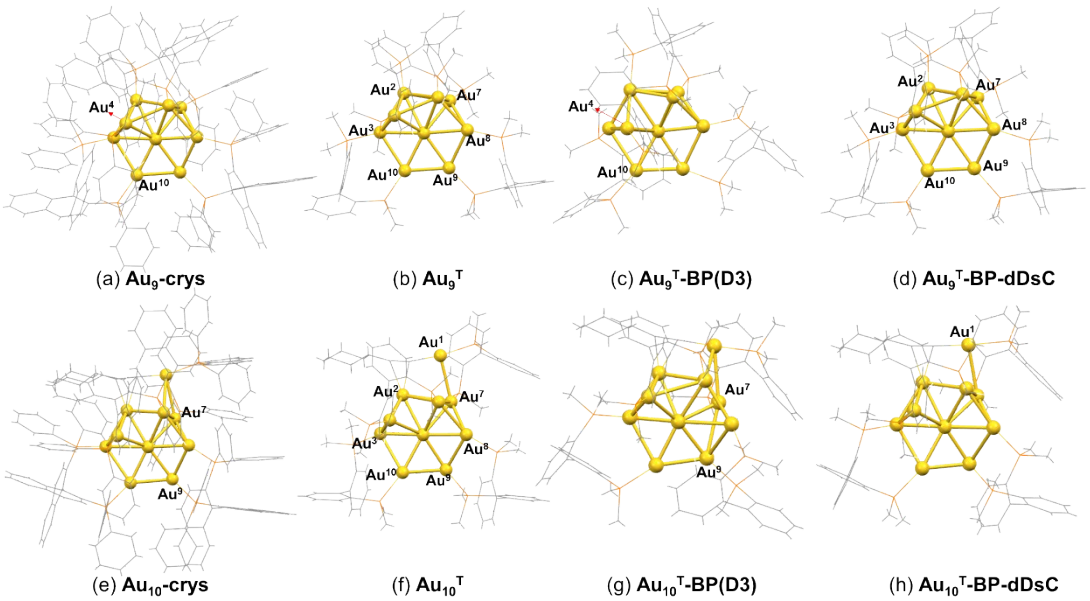

Figure S2. Comparison of the single crystal structure ($\mathbf{Au_9^T}$/$\mathbf{Au_{10}^T}$) and the optimized geometries of $\mathbf{Au_9^T}$/$\mathbf{Au_{10}^T}$ calculated with BP, BP-D3(BJ) and BP-dDsC functions.

Table S2. Some structural parameters of single crystal structure of Au_{10}/Au_9 and parameters of optimized geometries of $\mathbf{Au_{10}^T}$/$\mathbf{Au_9^T}$ calculated with BP, BP-D3(BJ) and BP-dDsC functions.

	$BD^{4\text{-}10}$	$BD^{7\text{-}9}$	$DA^{8\text{-}9\text{-}10\text{-}3}$	$DA^{7\text{-}8\text{-}9\text{-}10}$	$DA^{3\text{-}2\text{-}7\text{-}8}$	$DA^{10\text{-}3\text{-}2\text{-}7}$
Au_{10}-crys	3.926	3.930	41.8	285.0	287.3	31.3
Au_{10}^T	3.911	4.307	58.0	283.9	299.7	38.5
Au_{10}^T-BP(D3)	4.394	3.089	57.4	262.6	281.3	18.5
Au_{10}^T-BP-dDsC	3.973	3.885	60.3	272.9	291.8	32.5
Au_9-crys	4.138	4.130	29.6	296.9	296.7	21.4
Au_9^T	4.287	4.302	20.7	303.5	299.5	17.2
Au_9^T-BP(D3)	3.360	4.535	32.7	307.8	285.9	49.6
Au_9^T-BP-dDsC	4.268	4.253	23.8	301.5	301.4	16.6

Note: The Au-Au bond distances ($BD^{a\text{-}b}$) and dihedral angles ($DA^{a\text{-}b\text{-}c\text{-}d}$) are given in angstrom and degree, respectively.

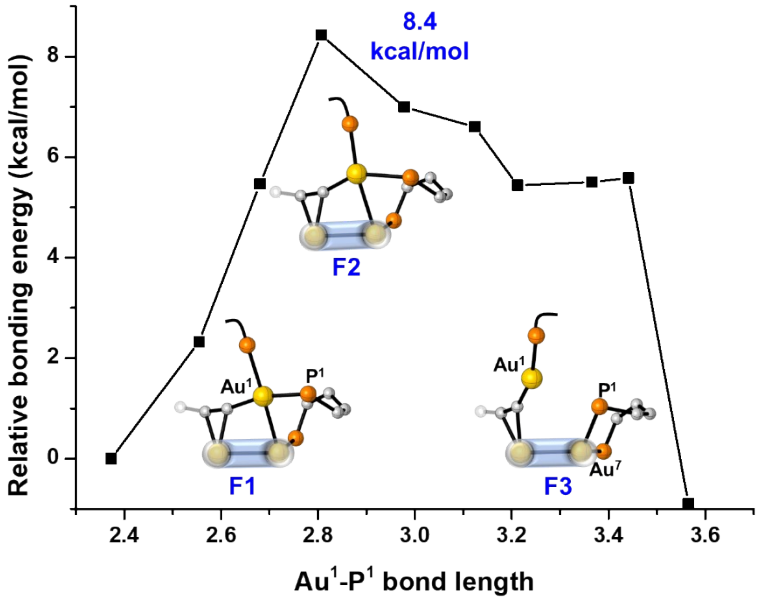

Figure S3. Partial optimization by fixing the Au^1-P^1 bond length at different values (from 2.373 Å in $\mathbf{Au_{10}^T}$**-I1** to 3.565 Å in $\mathbf{Au_{10}^T}$**-I3**). The relative bonding energies are given in kcal/mol, and the relative energy of **F1** is set as the reference.

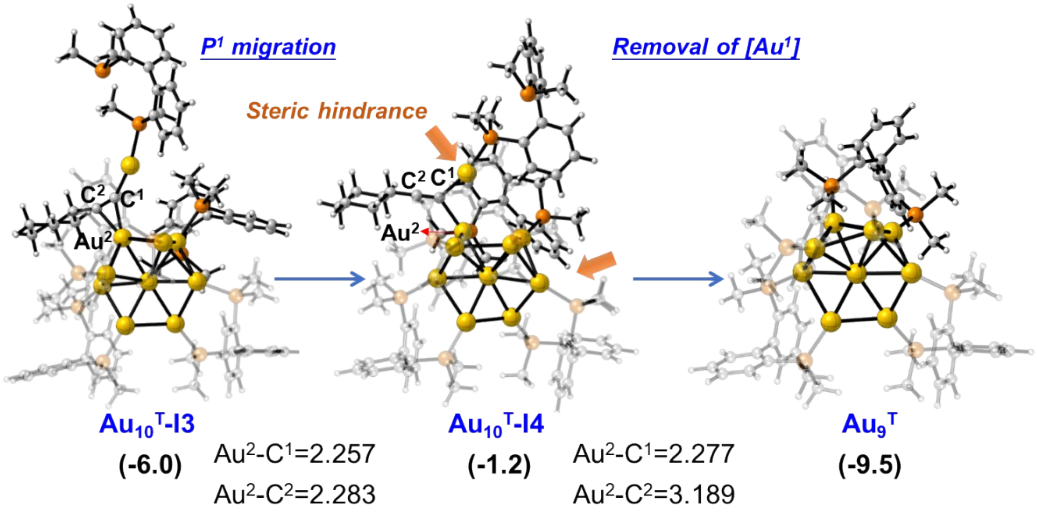

Figure S4. The optimized geometry and relative bonding energy (in kcal/mol) of $\mathbf{Au_{10}^T}$**-I3**, $\mathbf{Au_{10}^T}$**-I4** and $\mathbf{Au_9^T}$. The orange arrow illustrates the steric hindrance between the exterior ligands. The selected bond distances are given in angstrom.

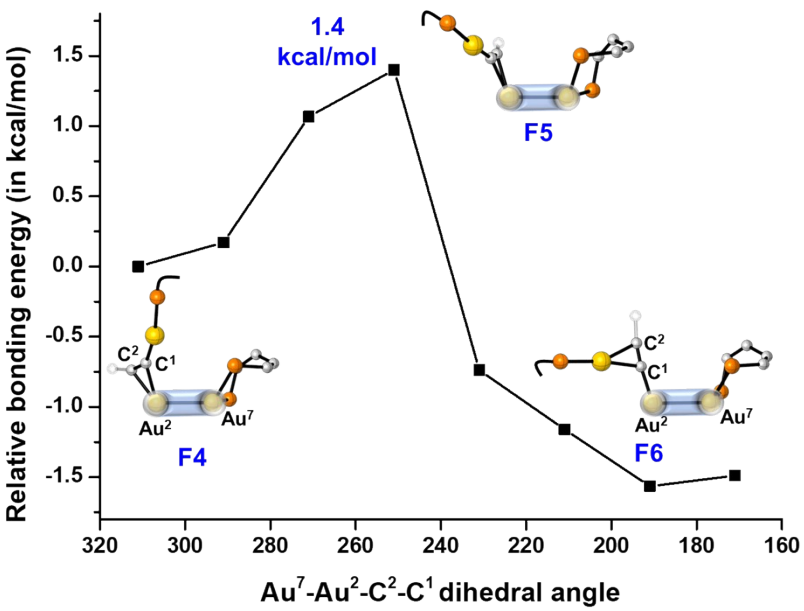

Figure S5. Partial optimization by fixing the Au^7-Au^2-C^2-C^1 dihedral angle at different values (from 310.8° in $\mathbf{Au_{10}^T}$**-I3** to 171.2° in $\mathbf{Au_{10}^T}$**-I5**). The relative bonding energies are given in kcal/mol, and the relative energy of **F4** is set as the reference. **F4** is optimization structure fixed at 310.8°, the relative energy is 0.2 kcal/mol higher than that of $\mathbf{Au_{10}^T}$**-I3**.

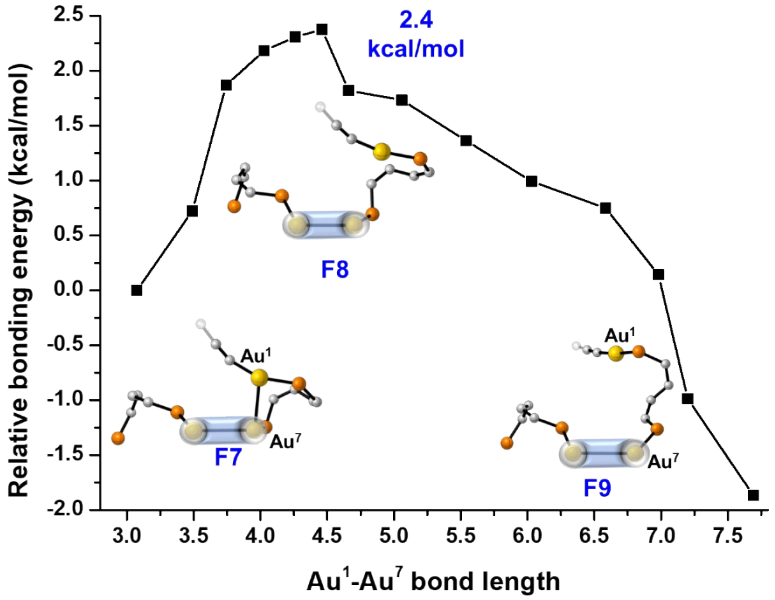

Figure S6. Partial optimization by fixing the Au^1-Au^7 bond length at different values (from 3.075 Å in $\mathbf{Au_{10}^T}$**-I7** to 7.694 Å in $\mathbf{Au_{10}^T}$**-I8**). The relative bonding energies are given in kcal/mol, and the relative energy of **F7** is set as the reference.

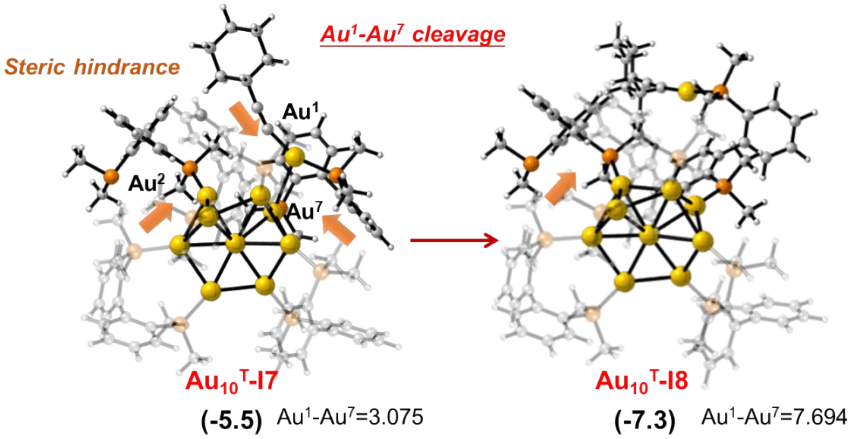

Figure S7. The optimized geometry and relative bonding energy (in kcal/mol) of **Au_{10}^{T}-I7** and **Au_{10}^{T}-I8**. The orange arrow illustrates the steric hindrance between the exterior ligands. The selected bond distances are given in angstrom.

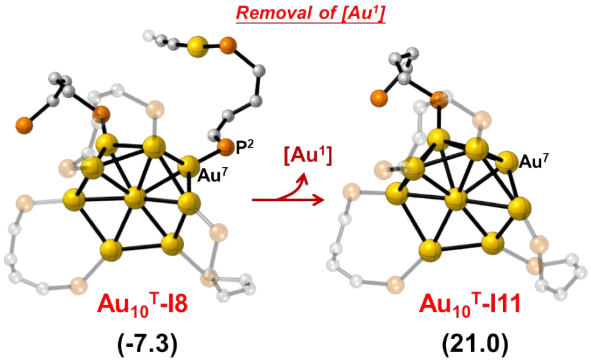

Figure S8. The optimized geometry and the relative bonding energies (in kcal/mol) after the removal of [Au^1] from **Au_{10}^{T}-I8**. For clarity, all hydrogen atoms in optimized geometries are omitted, and only one carbon atom of the cyclohexyl group on C^2 atom is shown.

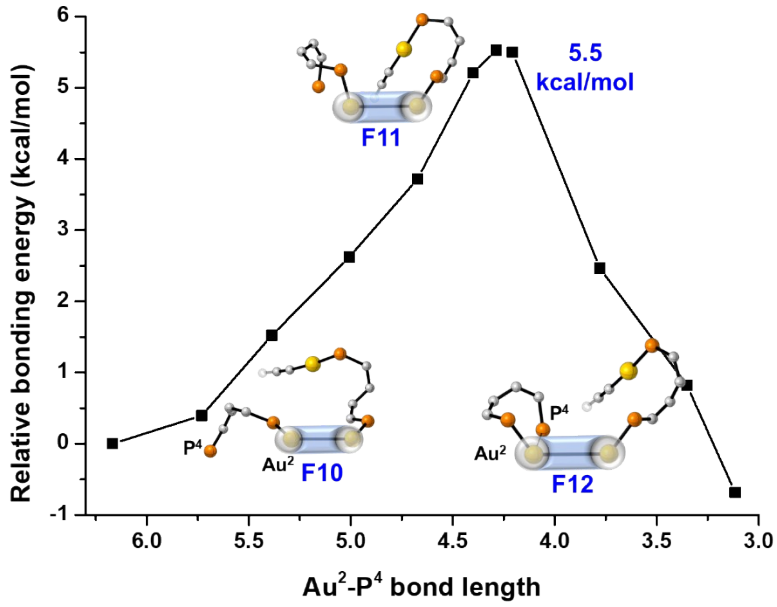

Figure S9. Partial optimization by fixing the Au^2-P^4 bond length at different values (from 6.169 Å in **Au_{10}^T-I8** to 3.116 Å in **Au_{10}^T-I9**). The relative bonding energies are given in kcal/mol, and the relative energy of **F10** is set as the reference.

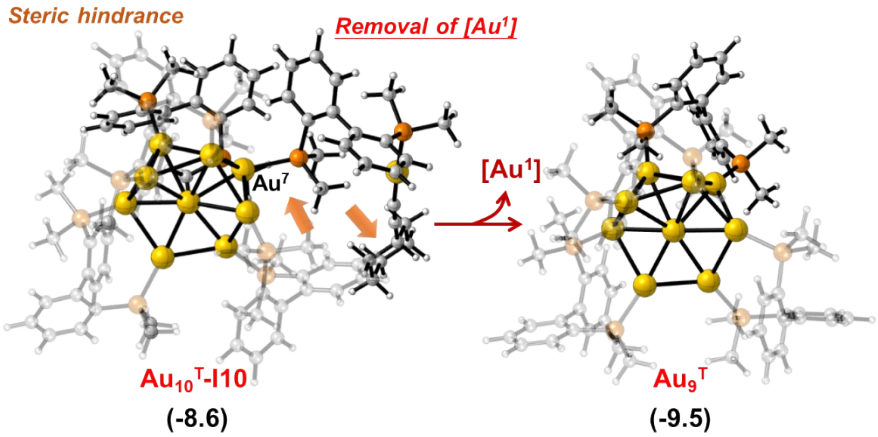

Figure S10. The optimized geometry and relative bonding energy (in kcal/mol) of **Au_{10}^T-I10** and **Au_9^T**. The orange arrow illustrates the steric hindrance between the exterior ligands.

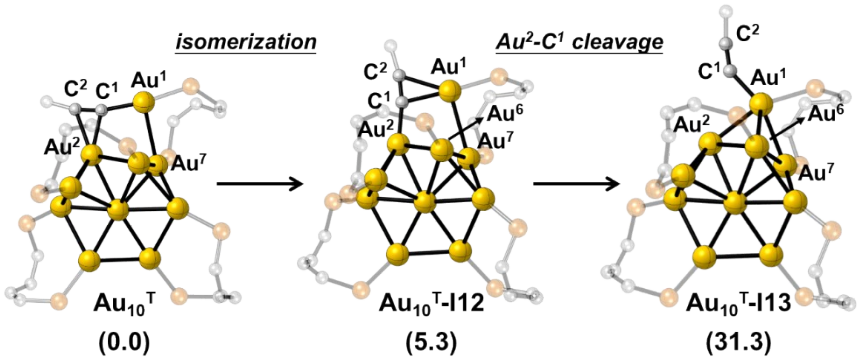

Figure S11. The removal of the Au^1-alkyne group from **Au_{10}^T** via the cleavage of Au^2-

alkyne. The relative bonding energies are given in kcal/mol.

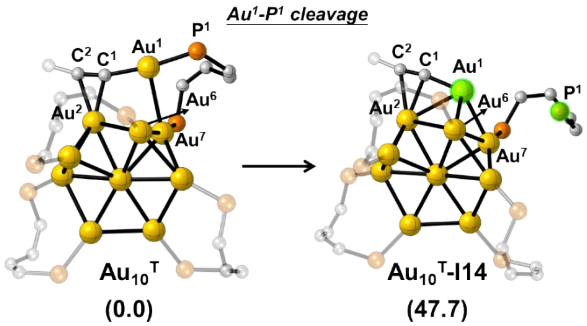

Figure S12. The removal of the Au[1]-alkyne group from $\mathbf{Au_{10}^T}$ via the cleavage of Au[1]-P[1]. The relative bonding energies are given in kcal/mol.

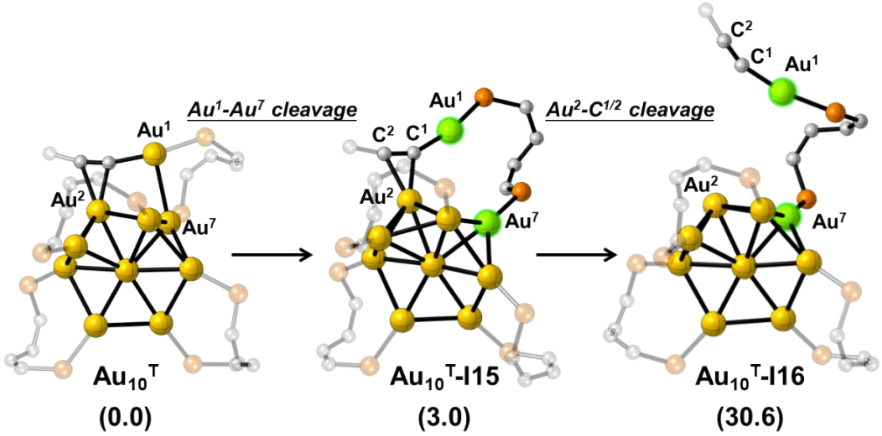

Figure S13. The removal of the Au[1]-alkyne group from $\mathbf{Au_{10}^T}$ via the cleavage of Au[1]-Au[7]. The relative bonding energies are given in kcal/mol.

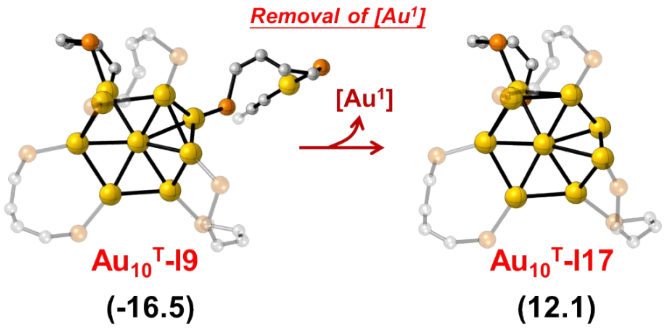

Figure S14. The optimized geometry and the relative bonding energies (in kcal/mol) after the removal of [Au[1]] from $\mathbf{Au_{10}^T}$**-I9**.

Table S3. Entropy and approximate Gibbs free energy of $\mathbf{Au_{10}^T}$**-I9** and $\mathbf{Au_9^T}$.

	Bond energy(kcal/mol)	Entropy(cal/mole-K)	ΔG(kcal/mol)
$\mathbf{Au_{10}^T}$	-23568.06	546.177	
$\mathbf{Au_{10}^T}$**-I9**	-28737.07	616.265	-1.08
$\mathbf{Au_9^T}$	-20980.84	494.570	-10.9

DMPP	-5152.55	121.674
DMPP-CCAu	-7749.31	177.907

Note: The temperature used in our calculation is 298.15K. G=H-TS, we use bond energy to estimate enthalpy to calculate Gibbs free energy. DMPP-CCAu is the Au-alkyne-DMPP moiety. The reaction equation: Au_{10}^{T}+DMPP→Au_{9}^{T}+DMPP-CCAu.

Table S4. Different methods calculate the intermediates and transition state of the conversion of **Au_{10}^{T}** to **Au_{9}^{T}** through Path II.

	BP	PBE	TPSS
Au_{10}^{T}	0.0	0.0	0.0
Au_{10}^{T}-I2	-0.9	-7.7	-4.3
Au_{10}^{T}-I7	-5.5	-11.7	-7.0
Au_{10}^{T}-$TS^{F(7-8)}$	-3.1	-8.1	-4.0
Au_{10}^{T}-I8	-7.3	-10.2	-7.4
Au_{10}^{T}-$TS^{F(8-9)}$	-1.8	-6.5	-3.6
Au_{10}^{T}-I9	-16.5	-21.2	-16.2
Au_{10}^{T}-$TS^{(9-10)}$	0.6	-4.6	-1.0
Au_{10}^{T}-I10	-8.6	-15.3	-9.8
Au_{9}^{T}	-9.5	-11.8	-9.8

Note: Geometry optimization was conducted with the GGA: BP functional, based on the optimized geometries, the solution phase single point energy calculations were carried out with COSMO model and different methods (such as PBE and TPSS).

Table S5. The Hirshfeld charge on Au atoms of **Au_{10}^{T}** and **Au_{10}^{T}-I2** calculated by different methods.

Au_{10}^{T}	Au^{1}	Au^{2}	Au^{3}	Au^{4}	Au^{5}	
BP	0.113	0.089	0.010	0.032	-0.046	-
PBE	0.119	0.092	0.013	0.037	-0.047	-
TPSS	0.127	0.089	0.012	0.037	-0.052	-
Au_{10}^{T}	Au^{6}	Au^{7}	Au^{8}	Au^{9}	Au^{10}	Au^{sum}
BP	0.012	0.014	0.002	-0.012	-0.007	0.207
PBE	0.015	0.017	0.005	-0.008	-0.003	0.240
TPSS	0.015	0.017	0.005	-0.01	-0.004	0.236
Au_{10}^{T}-I2	Au^{1}	Au^{2}	Au^{3}	Au^{4}	Au^{5}	
BP	0.125	0.080	0.012	0.015	-0.051	-
PBE	0.130	0.082	0.015	0.020	-0.052	-
TPSS	0.136	0.084	0.013	0.019	-0.057	-
Au_{10}^{T}-I2	Au^{6}	Au^{7}	Au^{8}	Au^{9}	Au^{10}	Au^{sum}
BP	0.010	0.008	0.007	-0.013	-0.008	0.185
PBE	0.013	0.011	0.011	-0.009	-0.004	0.217
TPSS	0.012	0.010	0.009	-0.010	-0.006	0.210

Note: Au^{sum} is the total charge of Au core of **Au_{10}^{T}** and **Au_{10}^{T}-I2**.

Table S6. The Hirschfeld charge of all Au atoms of $\mathbf{Au_9^T}$ and $\mathbf{Au_{10}^T}$.

	Au^1	Au^2	Au^3	Au^4	Au^5
In $\mathbf{Au_9^T}$	-	0.007	0.001	0.011	-0.049
In $\mathbf{Au_{10}^T}$	0.113	0.089	0.01	0.032	-0.046
	Au^6	Au^7	Au^8	Au^9	Au^{10}
In $\mathbf{Au_9^T}$	0.008	0.011	0.002	-0.011	-0.010
In $\mathbf{Au_{10}^T}$	0.012	0.014	0.002	-0.012	-0.007

Note: The total charge of all Au atoms in $\mathbf{Au_{10}^T}$/$\mathbf{Au_9^T}$ are 0.207 and -0.030 respectively. the charge of 5thDMPP in $\mathbf{Au_{10}^T}$**-I1**/$\mathbf{Au_{10}^T}$**-I2** are 0.213 and 0.327, demonstrating the electron-donating effect of the 5thDMPP. The sum of all atoms of $C_6H_{11}C{\equiv}CAu$ moiety of $\mathbf{Au_9^T}$**-I1** is -0.242, demonstrating a significant electron-withdrawing effect of the $C_6H_{11}C{\equiv}CAu$ complex.

Table S7. The different types of charge of Au atoms in the Au core of $\mathbf{Au_{10}^T}$/$\mathbf{Au_9^T}$.

In $\mathbf{Au_{10}^T}$	Au^1	Au^2	Au^3	Au^4	Au^5	Au^6	Au^7	Au^8	Au^9	Au^{10}
Hirschfeld	0.113	0.089	0.01	0.032	-0.046	0.012	0.014	0.002	-0.012	-0.007
Mulliken	0.285	0.1	-0.049	-0.003	-0.031	-0.04	-0.061	-0.046	-0.07	-0.047
Bader	0.065	0.06	-0.101	-0.082	-0.108	-0.118	-0.1	-0.112	-0.113	-0.111
In $\mathbf{Au_9^T}$	Au^1	Au^2	Au^3	Au^4	Au^5	Au^6	Au^7	Au^8	Au^9	Au^{10}
Hirschfeld	-	0.007	0.001	0.011	-0.049	0.008	0.011	0.002	-0.011	-0.01
Mulliken	-	-0.005	-0.05	-0.026	-0.066	-0.007	-0.031	-0.045	-0.058	-0.054
Bader	-	-0.109	-0.126	-0.104	-0.127	-0.106	-0.109	-0.105	-0.107	-0.109

Note: The total Hischfeld, Mulliken and Bader charge of all Au atoms in $\mathbf{Au_{10}^T}$ are 0.207, 0.038 and -0.72 respectively. And the total Hischfeld, Mulliken and Bader charge of all Au atoms in $\mathbf{Au_9^T}$ are -0.03, -0.342 and -1.002 respectively.

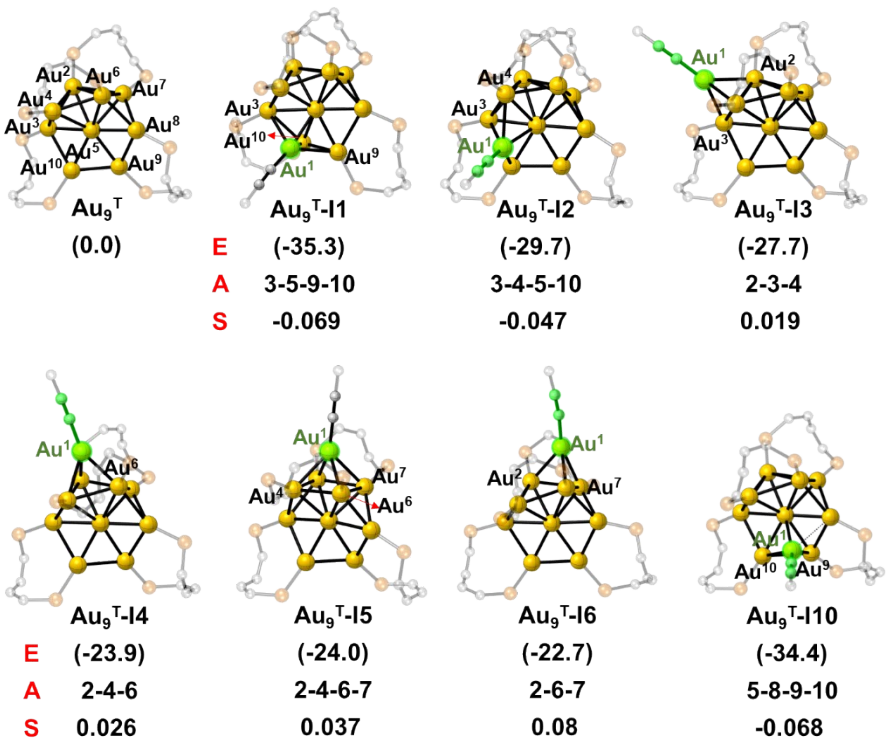

Figure S15. The relative bonding energy of different structures formed by the binding of {Au[1]} on different blocks. The relative energy of **Au$_9^T$** was set as the reference. E: relative bond energy; A: bonding atoms; S: sum of Hirschfeld charges of the bonding atoms in **Au$_9^T$**.

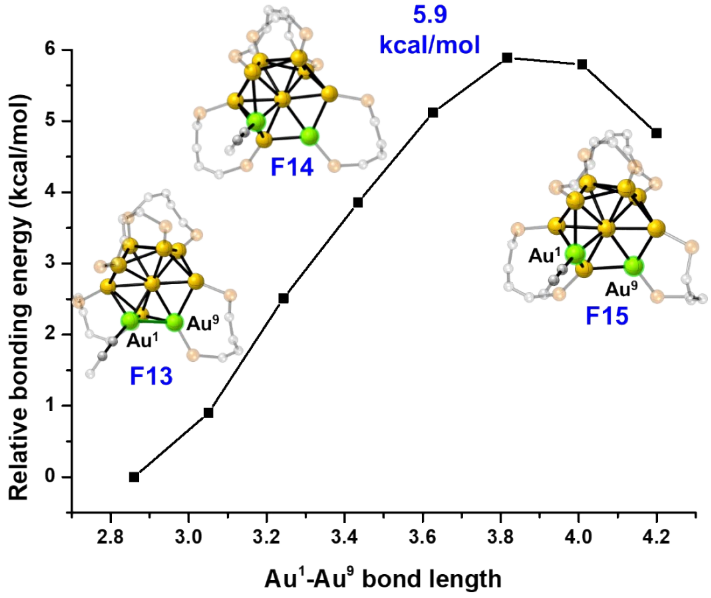

Figure S16. Partial optimization by fixing the Au[1]-Au[9] bond length at different values (from 2.860 Å in **Au$_9^T$-I1** to 4.200 Å in **Au$_9^T$-I2**). The relative bonding energies are given in kcal/mol, and the relative energy of **F13** is set as the reference.

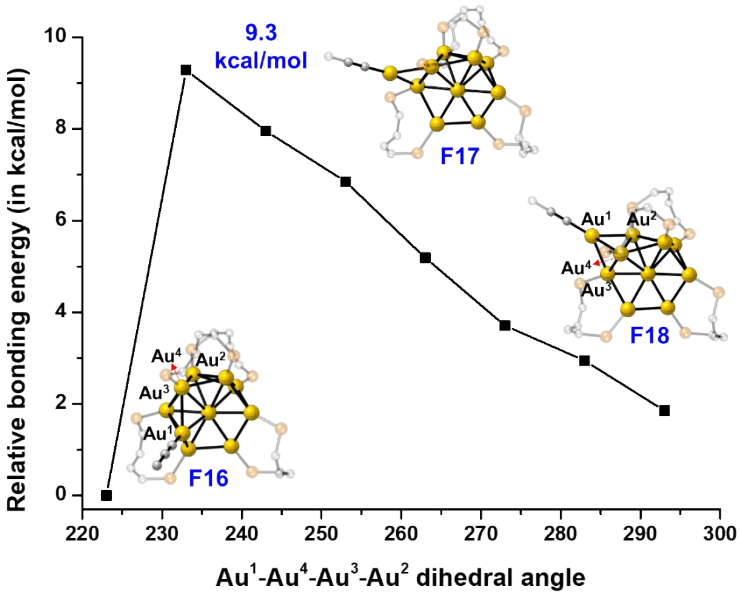

Figure S17. Partial optimization by fixing the Au^1-Au^4-Au^3-Au^2 dihedral angle at different values (from 223.1° in **Au_9^T-I2** to 293.0° in **Au_9^T-I3**). The relative bonding energies are given in kcal/mol, and the relative energy of **F16** is set as the reference.

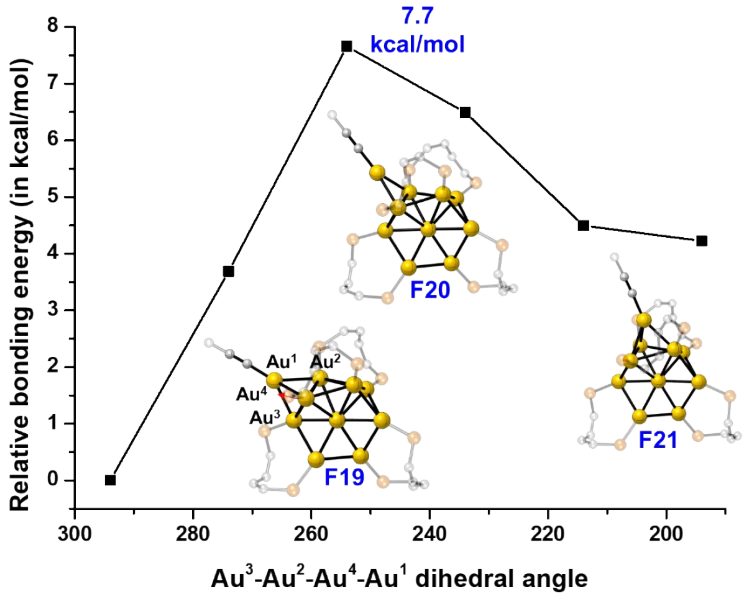

Figure S18. Partial optimization by fixing the Au^3-Au^2-Au^4-Au^1 dihedral angle at different values (from 294.0° in **Au_9^T-I3** to 194.0° in **Au_9^T-I4**). The relative bonding energies are given in kcal/mol, and the relative energy of **F19** is set as the reference.

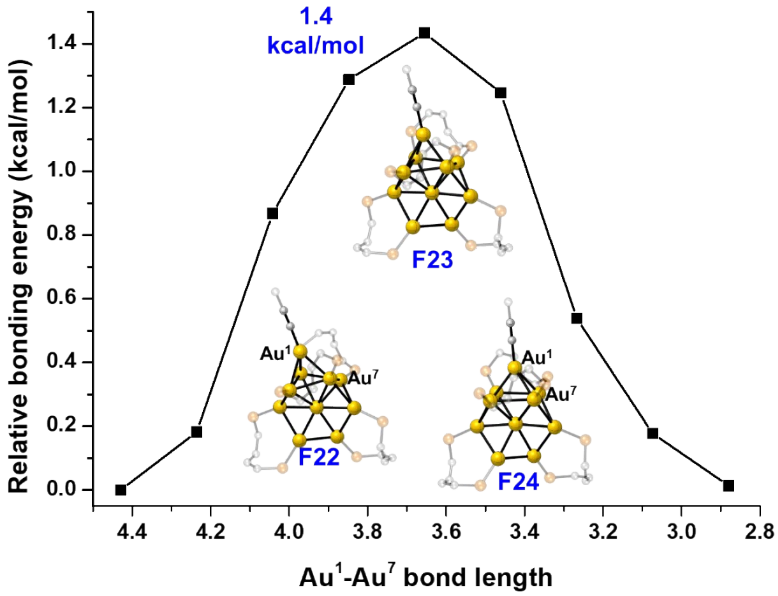

Figure S19. Partial optimization by fixing the Au^1-Au^7 bond length at different values (from 4.429 Å in **Au_9^T-I4** to 2.880 Å in **Au_9^T-I5**). The relative bonding energies are given in kcal/mol, and the relative energy of **F22** is set as the reference.

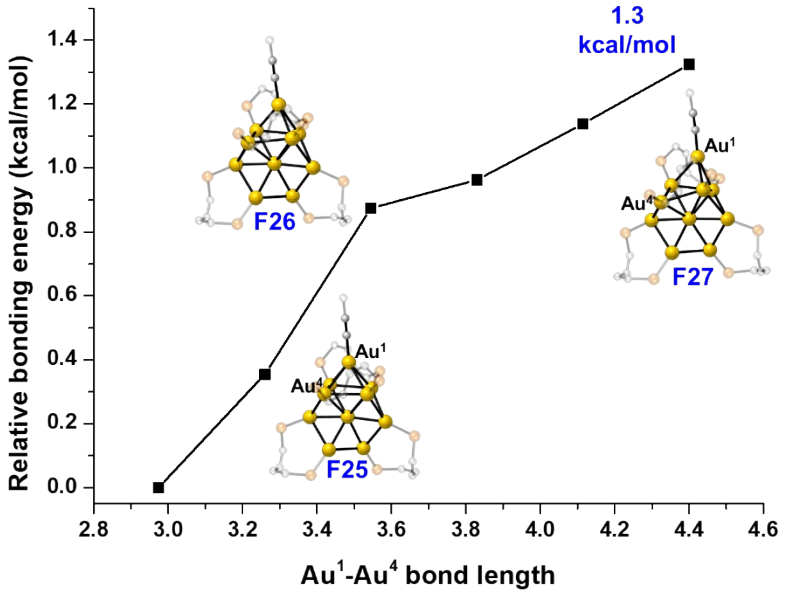

Figure S20. Partial optimization by fixing the Au^1-Au^4 bond length at different values (from 2.974 Å in **Au_9^T-I5** to 4.400 Å in **Au_9^T-I6**). The relative bonding energies are given in kcal/mol, and the relative energy of **F25** is set as the reference.

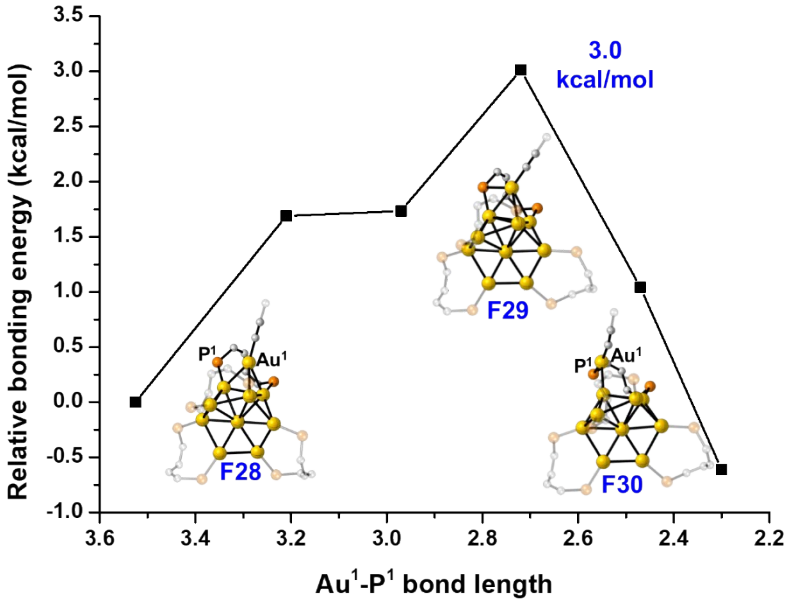

Figure S21. Partial optimization by fixing the Au^1-P^1 bond length at different values (from 3.525 Å in $\mathbf{Au_9^T}$**-I6** to 2.300 Å in $\mathbf{Au_9^T}$**-I7**). The relative bonding energies are given in kcal/mol, and the relative energy of **F28** is set as the reference.

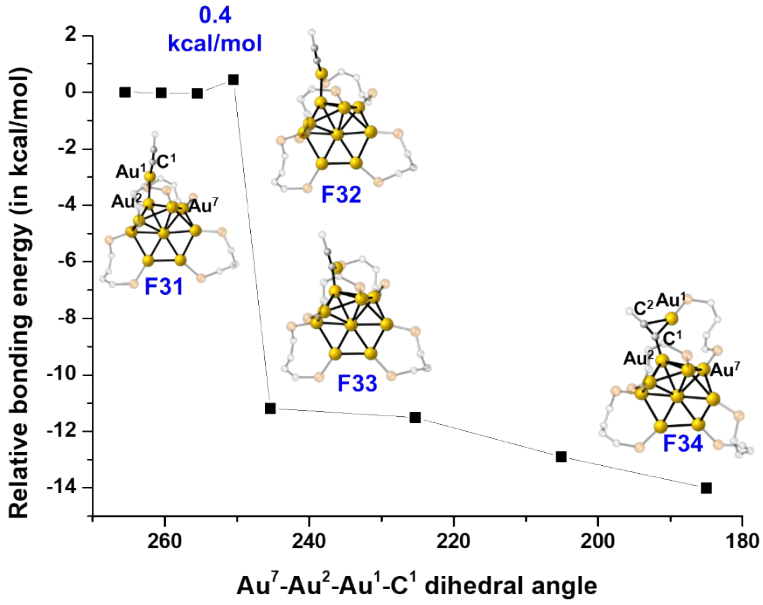

Figure S22. Partial optimization by fixing the Au^7-Au^2-Au^1-C^1 dihedral angle at different values (from 265.5° in $\mathbf{Au_9^T}$**-I7** to 185.0° in $\mathbf{Au_9^T}$**-I8**). The relative bonding energies are given in kcal/mol, and the relative energy of **F31** is set as the reference.

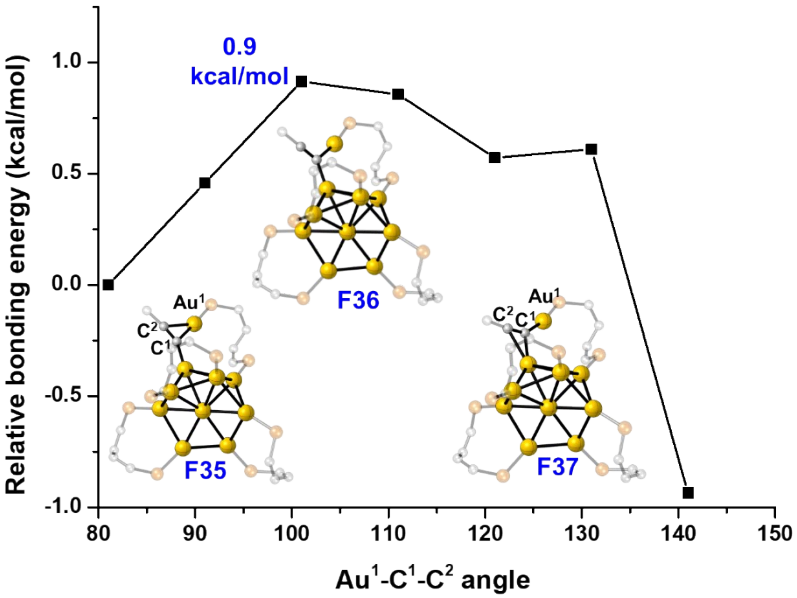

Figure S23. Partial optimization by fixing the Au^1-C^1-C^2 angle at different values (from 81.0° in **Au_9^T-I8** to 141.0° in **Au_9^T-I9**). The relative bonding energies are given in kcal/mol, and the relative energy of **F35** is set as the reference.

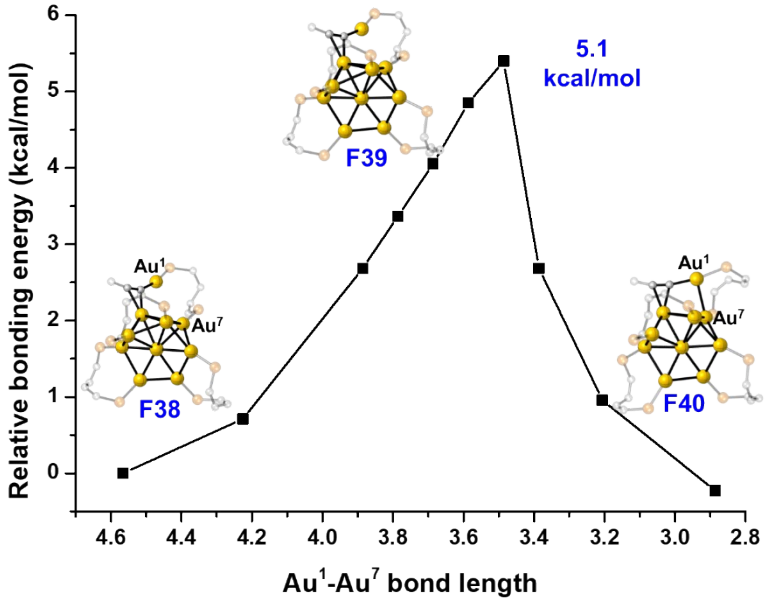

Figure S24. Partial optimization by fixing the Au^1-Au^7 bond length at different values (from 4.556 Å in **Au_9^T-I9** to 2.886 Å in **Au_{10}^T**). The relative bonding energies are given in kcal/mol, and the relative energy of **F38**is set as the reference.

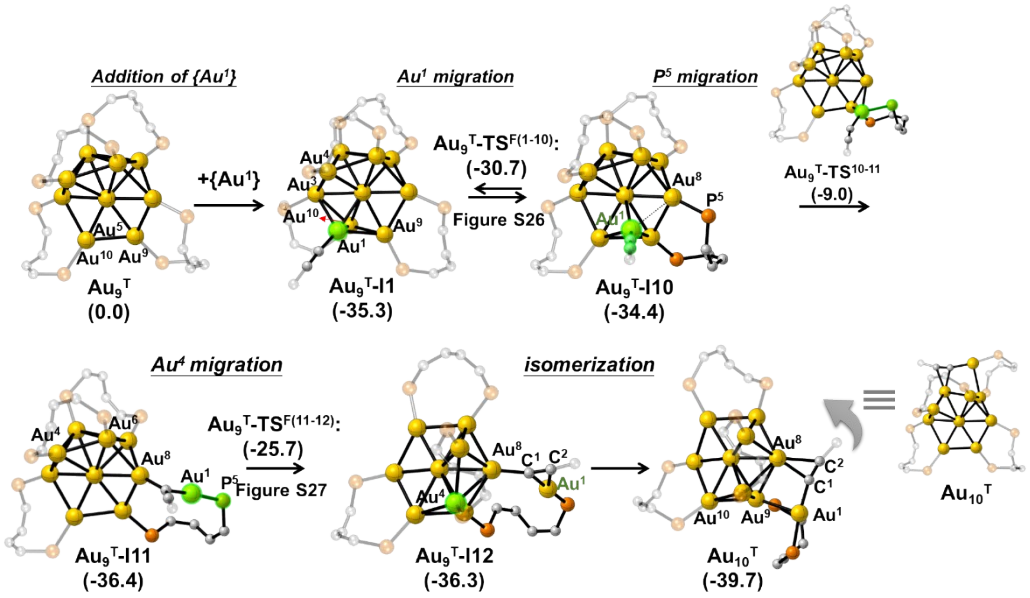

Figure S25. The optimized geometry and the relative bonding energies (in kcal/mol) for the transformation from **Au_9^T** to **Au_{10}^T** via alternative {Au^1} migration pathway.

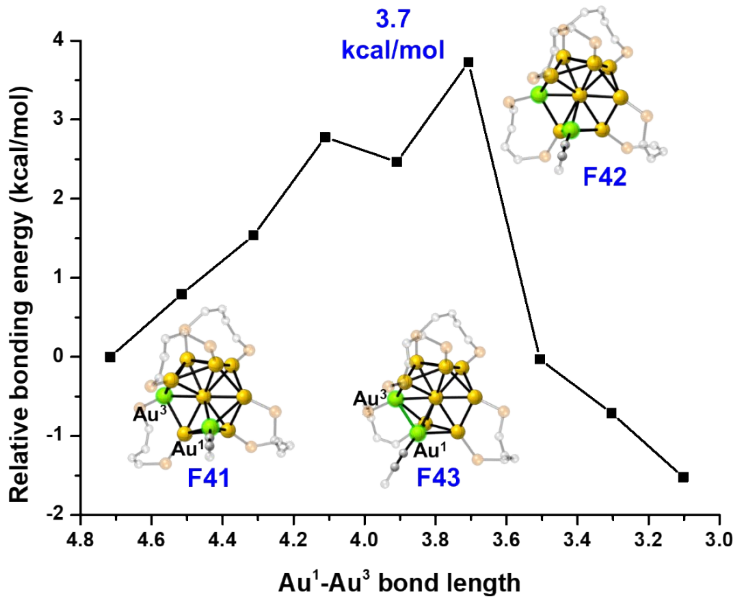

Figure S26. Partial optimization by fixing the Au^1-Au^3 bond length at different values (from 4.716 Å in **Au_9^T-I10** to 2.900 Å in **Au_9^T-1**). The relative bonding energies are given in kcal/mol, and the relative energy of **F41** is set as the reference.

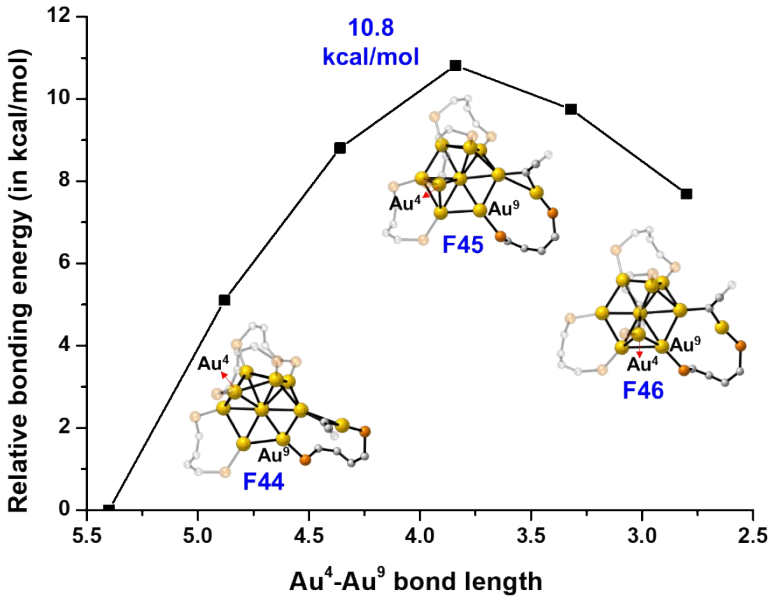

Figure S27. Partial optimization by fixing the Au^4-Au^9 bond length at different values (from 5.400 Å in **Au_9^T-I11** to 2.800 Å in **Au_9^T-I12**). The relative bonding energies are given in kcal/mol, and the relative energy of **F44**is set as the reference.

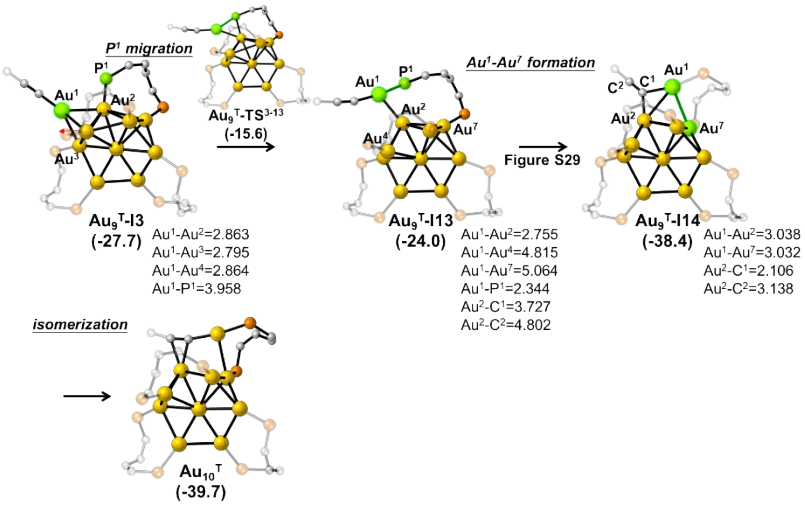

Figure S28. The optimized geometry and the relative bonding energies (in kcal/mol) for phosphine migration on **Au_9^T-I3**.

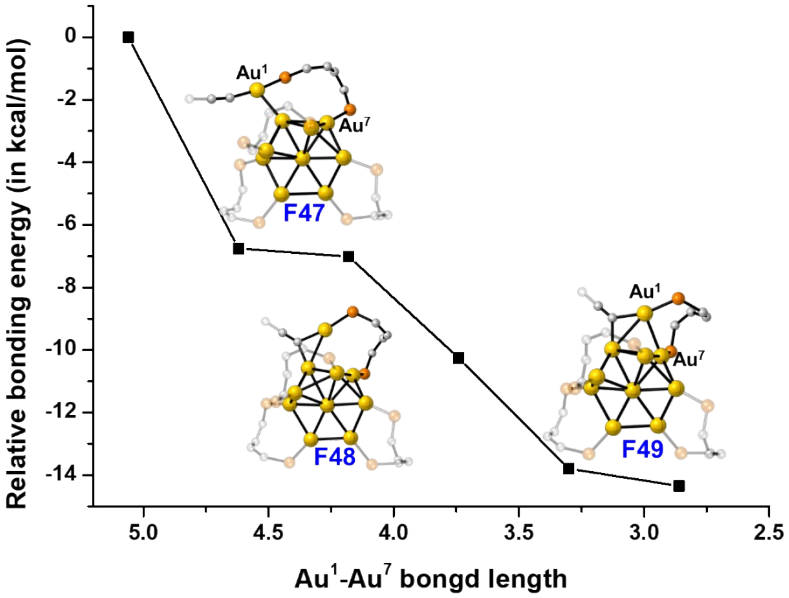

Figure S29. Partial optimization by fixing the Au^1-Au^7 bond length at different values (from 5.060 Å in **Au_9^T-I13** to 2.860 Å in **Au_9^T-I14**). The relative bonding energies are given in kcal/mol, and the relative energy of **F47** is set as the reference.

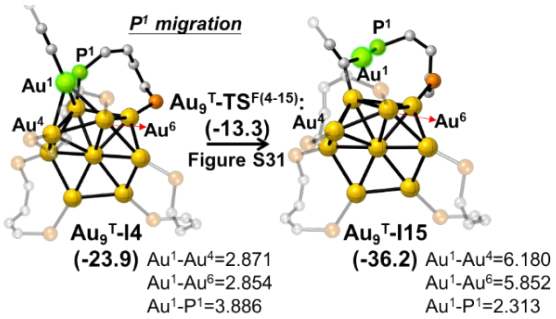

Figure S30. The optimized geometry and the relative bonding energies (in kcal/mol) for phosphine migration on **Au_9^T-I4**.

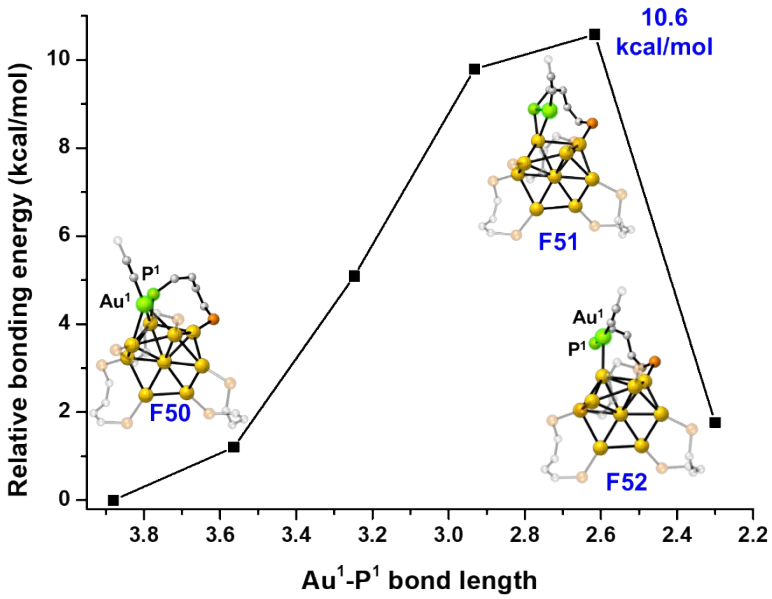

Figure S31. Partial optimization by fixing the Au^1-P^1 bond length at different values (from 3.880 Å in **Au_9^T-I4** to 2.300 Å in **Au_9^T-I15**). The relative bonding energies are given in kcal/mol, and the relative energy of **F50** is set as the reference.

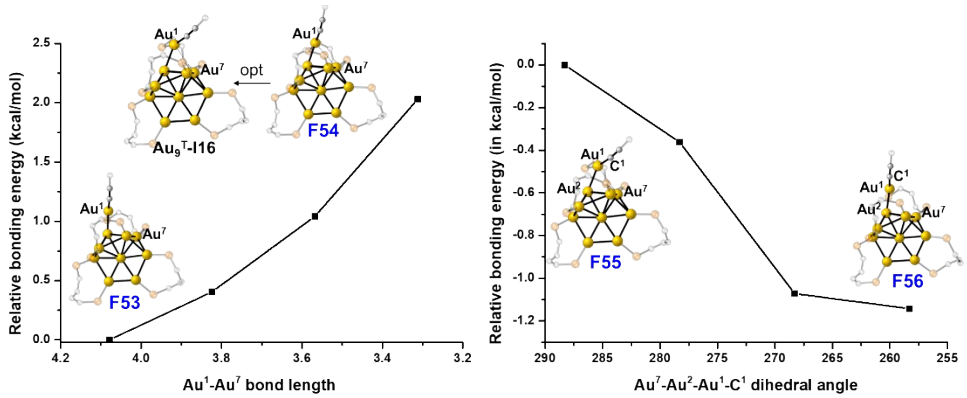

Figure S32. The Au^1-Au^7 bond formation induced conversion of **Au_9^T-I7** to **Au_{10}^T**. Left: the partial optimization by fixing the Au^1-Au^7 bond length at different values (from 4.079 Å in **Au_9^T-I13** to 3.312 Å in **F54**), **Au_9^T-I16** is the result of **F54** optimization. Right: the partial optimization by fixing the Au^7-Au^2-Au^1-C^1 dihedral angle at different values (from 288.3° in **Au_9^T-I16** to 258.3° in **F56**).